Acceleration Feedback in PID Controlled Elastic Drive Systems ⋆

Václav Helma,Martin Goubej,Ondřej Ježek

NTIS research centre, University of West Bohemia, Pilsen, Czechia
e-mail:{helma,mgoubej,ojezek}@ntis.zcu.cz

Abstract: This paper deals with the use of a load acceleration feedback to overcome fundamental performance limitations of elastic servo drive systems that occur when employing a standard PI velocity controller. Structured H-infinity optimization approach is used to develop an optimal control strategy consisting of a PI controller and a static acceleration feedback. Qualitative and quantitative analysis of potential benefits for the case of a two-mass system is provided. Effects of higher resonance modes is studied as well. Experimental results demonstrate the application of the proposed methodology to a flexible arm manipulator.

Keywords: vibration damping, PID controllers, acceleration feedback, motion control, drives

1. INTRODUCTION

Modern motion control systems rely on properly adjusted velocity and position feedback loops. Their accurate tuning is essential when dealing with stringent performance requirements. Although several advanced control strategies were proposed, the conventional cascade PID scheme still remains prevalent in industrial servo drives thanks to its simplicity, low number of parameters and fair performance in most situations.

One of the limiting factors which affect the achievable quality of control is a mechanical compliance of a driven load. Proper adjustment of the feedback control is necessary in order to cope with unwanted transient or residual oscillations. A key issue of elastic servo systems is the absence of a direct information about the behavior of the driven load. Only a motor-side feedback is often available making the stabilization of an oscillatory load difficult. This can be overcome by means of an observer combined with a proper feedback (Ji and Sul (1995),Katsura and Ohnishi (2007),Thomsen et al. (2011)). However, such solutions depend heavily on the fidelity of the plant model. Another option is to install an additional instrumentation providing a complementary feedback information (Szabat and Orlowska-Kowalska (2007)). A load attached accelerometer may be a suitable choice for a wide range of applications due to the low price, small dimensions and simple mounting. Successful applications of the acceleration feedback were reported for robotic manipulators (Axelsson et al. (2014), Nam et al. (2016)), machine tools feed drives (Zirn and Jaeger (2010), de Argandona et al. (2005)) or linear positioning stages (Watanabe et al. (2016)). However, the suggested control strategies require implementation of a customized algorithm directly in the drive firmware which cannot be done in industrial applications with the off-the-shelf hardware.

⋆ This work was supported from I-MECH project by ECSEL Joint Undertaking under grant agreement No 737453

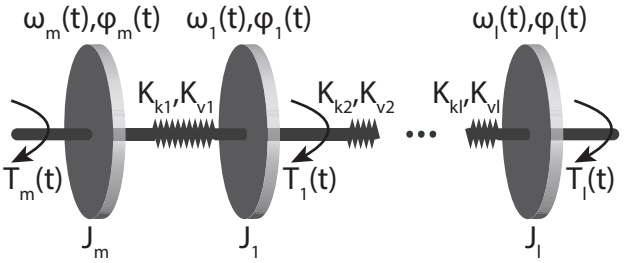

Fig. 1. Lumped multi-mass elastic drive system model

A natural effort is therefore to merge the benefits of using the auxiliary information with the simplicity of conventional PID control available in commercial drives. By introducing the auxiliary feedback, whether it is a motor acceleration (Zhang (2000); Goubej (2016)) or a motor-load reaction torque (Yuki et al. (1993); Katsura and Ohnishi (2007)), it is possible to shape the resonance ratio of the controlled system and achieve better performance. For the aforementioned reasons (low cost and small dimensions), it is again advantageous to use a MEMS accelerometer attached to the load. This acceleration feedback has a common features with the reaction torque feedback, as shown in Zhang (1999).

The paper is organised as follows. We begin with a definition of multi-mass flexible system models followed by a review of the achievable closed-loop performance valid for the PID controllers. Section 3 provides a brief summary of possible auxiliary feedbacks that can be used in servo-drive control. Section 4 is dedicated to a H_∞ optimal control. Analysis of reference tracking and disturbance rejection performance reveals potential benefits of the load-side acceleration feedback. The presence of a higher resonance mode and its impact on the closed-loop behaviour is also analyzed. The experimental results in Section 5 demonstrate the applicability of the proposed approach to a distributed parameter elastic system with multiple flexible modes.

© 2018 International Federation of Automatic Control

2. MATHEMATICAL MODEL

The starting point is a generic lumped-parameter model of a flexible mechanical system schematically illustrated in Figure 1. The motor and load dynamics is governed by transfer functions

$$P_n^m = \frac{\omega_m(s)}{T_m(s)} = \frac{K}{s}\prod_{i=1}^{n}\frac{s^2+2\xi_{zi}\omega_{zi}s+\omega_{zi}^2}{s^2+2\xi_{pi}\omega_{pi}s+\omega_{pi}^2}, \quad (1)$$

$$P_n^l = \frac{\omega_l(s)}{T_m(s)} = \frac{K}{s}\prod_{i=1}^{n}\frac{2\xi_{zi}\omega_{zi}s+\omega_{zi}^2}{s^2+2\xi_{pi}\omega_{pi}s+\omega_{pi}^2},$$

where K is an integration gain of the system, ξ_{pi} and ω_{pi} are the damping factors and natural frequencies of the complex poles belonging to the i-th resonance mode and ξ_{zi} and ω_{zi} are damping factors and natural frequencies of the i-th anti-resonance, $\omega_m(t) = \mathscr{L}^{-1}\{\omega_m(s)\}$ is a motor-side velocity, $\omega_l(t) = \mathscr{L}^{-1}\{\omega_l(s)\}$ is a load-side velocity and $T_m(t) = \mathscr{L}^{-1}\{T_m(s)\}$ is a motor torque.

A two-mass system is obtained as a special case for $n = 1$ leading to transfer functions

$$P_2^m(s) = \frac{\omega_m(s)}{T_m(s)} = \frac{J_l s^2 + K_v s + K_k}{s\left(J_m J_l s^2 + K_v(J_m+J_l)s + K_k(J_m+J_l)\right)} = \\ = \frac{K_1}{s}\cdot\frac{s^2+2\xi_z\omega_z s+\omega_z^2}{s^2+2\xi_p\omega_p s+\omega_p^2}, \quad (2)$$

$$P_2^l(s) = \frac{\omega_l(s)}{T_m(s)} = \frac{K_v s + K_k}{s\left(J_m J_l s^2 + K_v(J_m+J_l)s + K_k(J_m+J_l)\right)} = \\ = \frac{K_2}{s}\cdot\frac{s+\frac{\omega_z}{2\xi_z}}{s^2+2\xi_p\omega_p s+\omega_p^2}, \quad (3)$$

where J_m, J_l are the moments of inertia of motor or load respectively, K_k and K_v denote the spring stiffness and damping. The corresponding gains, natural frequencies and damping factors can be expressed by means of the plant parameters as follows

$$K_1 = \frac{\omega_p^2}{(J_m+J_l)\omega_z^2}, \quad \omega_p = \sqrt{\frac{K_k(J_m+J_l)}{J_m J_l}}, \quad \omega_z = \sqrt{\frac{K_k}{J_l}},$$

$$K_2 = \frac{2\xi_z\omega_p^2}{J_m+J_l}, \quad \xi_p = \sqrt{\frac{K_v^2(J_m+J_l)}{4K_k J_m J_l}}, \quad \xi_z = \sqrt{\frac{K_v^2}{4K_k J_l}}. \quad (4)$$

Next, we assume a PI controller with the feedback introduced from the motor velocity

$$C_{PI}(s) = \frac{T_m(s)}{E(s)} = \frac{K_p s + K_i}{s}, \quad (5)$$

where K_p and K_i are the controller gains and $e(t) = \mathscr{L}^{-1}\{E(s)\}$ is the tracking error. The block diagram of this loop is shown in Figure 2. The damping terms K_v were omitted for the sake of clarity. However, they are considered in the following analysis.

As shown in Zhang (2000) and Goubej (2016), the fundamental property of the plant influencing the closed-loop performance is a so-called resonance ratio r or a corresponding drive to load inertia ratio R given as follows

$$r = \frac{\omega_p}{\omega_z} = \sqrt{1+\frac{J_l}{J_m}} = \sqrt{1+R}, \quad R = \frac{J_l}{J_m}. \quad (6)$$

Briefly, if the resonance ratio is small, the closed-loop response cannot be sufficiently damped. On the other hand, high resonance ratio leads to lower achievable bandwidth and excessive feedback gains. The best performance can be achieved if the resonance ratio is $r \approx 2$.

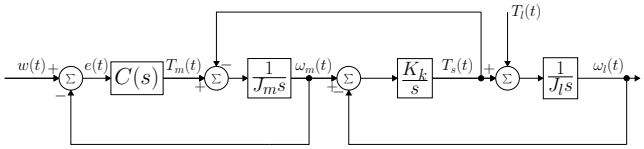

Fig. 2. Closed-loop block diagram

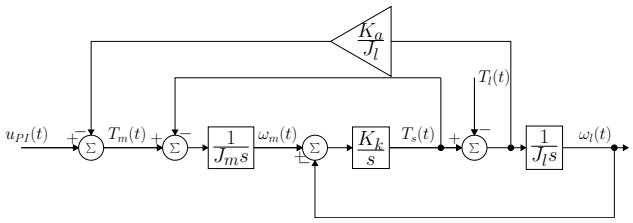

Fig. 3. Acceleration feedback diagram

For a general closed-loop analysis, it is further preferable to normalize the plant both in gain and time without loss of generality. This leads to the plant dynamics

$$P_{n2}^m(s) = \frac{r^2}{s}\cdot\frac{s^2+2\xi_z s+1}{s^2+2\xi_z r^2 s+r^2}, P_{n2}^l(s) = \frac{r^2}{s}\cdot\frac{2\xi_z s+1}{s^2+2\xi_z r^2 s+r^2}. \quad (7)$$

Similar approach is followed for the case of three-mass system which results to the normalized transfer functions

$$P_{n3}^m(s) = \frac{r_1^2 r_3^2}{s}\cdot\frac{(s^2+2\xi_{z1}s+1)(s^2+2\xi_{z2}r_1r_2s+r_1^2r_2^2)}{(s^2+2\xi_{p1}r_1s+r_1^2)(s^2+2\xi_{p2}r_1r_2r_3s+r_1^2r_2^2r_3^2)},$$

$$P_{n3}^l(s) = \frac{r_1^2 r_3^2}{s}\cdot\frac{(2\xi_{z1}s+1)(2\xi_{z2}r_1r_2s+r_1^2r_2^2)}{(s^2+2\xi_{p1}r_1s+r_1^2)(s^2+2\xi_{p2}r_1r_2r_3s+r_1^2r_2^2r_3^2)}, \quad (8)$$

where r_1 is the resonance ratio of the first flexible mode, r_2 is the second anti-resonance to first resonance frequency ratio and r_3 is the resonance ratio of the second flexible mode.

3. AUXILIARY FEEDBACK

Several papers outline some possibilities for introducing auxiliary feedback in order to virtually change the resonance ratio to enhance the closed-loop performance achievable with a standard PI controller (Zhang (1999)). One of the options (Goubej (2016)) is the utilization of the derivative action of the PID controller. However, this often requires a double differentiation of the motor position signal leading to a significant amplification of a high-frequency noise. Another alternative is to use the reaction torque feedback T_s. Nevertheless, this requires an expensive and bulky torque cell to be mounted in the drive system.

With the advances in the field of MEMS sensors, usage of an inexpensive load-attached accelerometer seems to be advantageous. The block diagram of this approach is shown in Figure 3 ($u_{PI}(t)$ denotes the output of the feedback controller). Such a structure has very similar properties to the torque sensor structure, it only differs in load disturbance (T_l) rejection.

If we now investigate the acceleration closed-loop dynamics we obtain

$$\frac{s\cdot\omega_l(s)}{u_{PI}(s)} = \frac{s\cdot P^l(s)}{1+K_a\cdot s\cdot P^l(s)} = \frac{K_1(2\xi_z\omega_z s+\omega_z^2)}{s^2+(\ldots)s+K_aK_1\omega_z^2+\omega_p^2}, \quad (9)$$

which implies that we can arbitrarily set the resonance ratio of this loop by adjusting the acceleration feedback gain

$$K_a = \frac{r^{w2} - r^2}{K_1}, \tag{10}$$

where r^w is the desired resonance ratio we want to achieve. We can conclude that we are able to virtually (from the PI controller perspective) change the resonance ratio of the plant by employing the acceleration feedback.

4. H_∞ OPTIMAL CONTROL AND ACHIEVABLE PERFORMANCE ANALYSIS

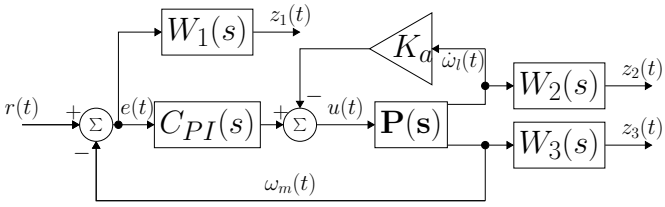

Fig. 4. Weighting scheme for the H_∞ controller synthesis

A weighting scheme from the Figure 4 is introduced for the single-input two-output plant

$$\mathbf{P(s)} = \begin{bmatrix} s \cdot P^l_{n2}(s) & P^m_{n2}(s) \end{bmatrix}^T, \tag{11}$$

formulating an optimal control design problem for the derivation of the PI controller parameters. Conventional control scheme without the acceleration feedback ($K_a = 0$) was considered for a first batch of experiments. The goal is to minimize the impact of the generalized input ($r(t)$) to penalized outputs ($z_1(t)$,$z_2(t)$) in the sense of the H_∞ norm of the closed-loop system

$$\|H\|_\infty = \left\| \begin{bmatrix} W_1(s) S^m_2(s) \\ W_2(s) \cdot s \cdot T^l_2(s) \end{bmatrix} \right\|_\infty \leq \gamma, \tag{12}$$

where $S^m_2(s)$ is the motor sensitivity function, $T^l_2(s)$ is the transfer function from the setpoint $r(t)$ to the load-side velocity $\omega_l(t)$ given by relations

$$S^m_2(s) = \frac{1}{1 + C_{PI}(s) P^m_{n2}(s)}, T^l_2(s) = \underbrace{(1 - S^m_2(s))}_{T^m_2(s)} \frac{P^l_{n2}(s)}{P^m_{n2}(s)}. \tag{13}$$

Following weighting functions which allow effective shaping of the corresponding closed-loop sensitivity functions are proposed

$$W_1(s) = \frac{\frac{1}{M_{sm}} s + \omega_1}{s + \frac{\omega_1}{A}}, W_2(s) = \frac{1}{s \cdot M_{tl}}. \tag{14}$$

The parameter A affects a low-frequency disturbance rejection. The value M_{sm} specifies a desired maximum sensitivity peak which is a direct measure of the robustness in stability. The cut-off frequency determined by ω_1 is related to the closed-loop bandwidth. The parameter M_{tl} is essentially the level of the load-side vibrations suppression.

The formulated structured H_∞ optimization was solved using the `hinfstruct` routine of the Matlab Robust Control Toolbox. Figure 5 shows the closed-loop performance achieved with the optimal controller for the weight parameters $M_{sm} = M_{tl} = 1.5, A = 1000$ and varying resonance ratio r of the normalized system. The cut-off frequency ω_1 was chosen as the highest possible value which leads to

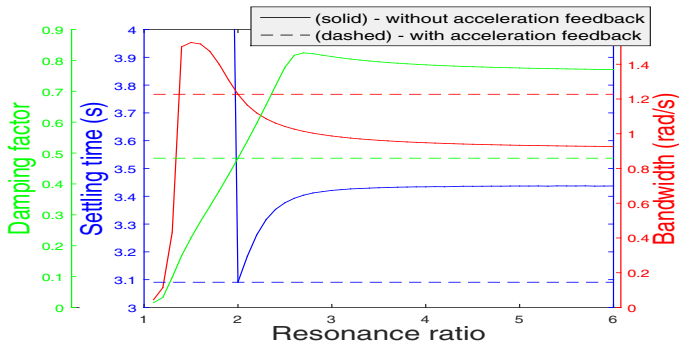

Fig. 5. Closed-loop performance as a function of the resonance ratio

a controller fulfilling the design requirements ($\gamma \leq 1$). The damping factor of normalized system was set to $\xi_z = 0.01$. The displayed bandwidth of $T^l_2(s)$ is defined in the standard -3dB sense

$$\left|T^l_2(jw)\right| > -3dB \quad \forall \omega \in < 0, \omega_{bw} > . \tag{15}$$

A dependency of the step response settling time with respect to the resonance ratio is shown as well. The settling time t_{st} is defined for the 2.5% steady state error tolerance

$$\left|g_l(t) - T^l_2(0)\right| < 0.025 \cdot T^l_2(0) \quad \forall t \in < t_{st}, \infty >, \tag{16}$$

$$g_l(t) = \mathscr{L}^{-1} \left\{ \frac{T^l_2(s)}{s} \right\}.$$

A minimum achieved damping factor of the closed-loop characteristic polynomial is also shown in Figure 5 to demonstrate a disturbance rejection performance. If we denote p_i as the i-th root of the characteristic polynomial, we can define a minimum damping factor as

$$\xi_{min} = \min_i \{ -\cos(\angle p_i) \}. \tag{17}$$

It can be seen that even the optimal controller is unable to provide a sufficient damping for low resonance ratios whereas high-resonance ratios lead to sluggish closed-loop response. These results are in coincidence with former analysis provided in (Zhang (2000); Goubej (2016)) using a modal control approach.

A second batch of experiments was performed for the acceleration feedback enhanced compensator. The weighting scheme has to be adjusted since the weights (14) tend to produce undesirable high gains. Therefore, a third generalized output $z_3(t)$ is introduced leading to the search for the controller gains $\{K_p, K_i, K_a\}$ by minimizing

$$\|H\|_\infty = \left\| \begin{bmatrix} W_1(s) S^{ma}_2(s) \\ W_2(s) \cdot s \cdot T^{la}_2(s) \\ W_3(s) T^{ma}_2(s) \end{bmatrix} \right\|_\infty \leq \gamma, \tag{18}$$

where $S^{ma}_2(s)$, $T^{la}_2(s)$ are the velocity sensitivity functions with the inner acceleration closed-loop defined in a similar way to (13), $T^{ma}_2(s) = (1 - S^{ma}_2(s))$ is the transfer function from the setpoint $r(t)$ to the motor-side velocity $\omega_m(t)$.

The weights $W_1(s)$ and $W_2(s)$ remain unchanged and the weight $W_3(s)$ penalizing the control effort is chosen as

$$W_3(s) = \frac{s + \frac{\omega_3}{M_{tm}}}{\frac{1}{A} s + \omega_3}. \tag{19}$$

If we now suitably move both cut-off frequencies ω_1 and ω_3 against each other until we reach $\gamma \approx 1$, we find that the optimal acceleration gain K_a smoothly converges to a value which shifts the virtual resonance ratio to the value of $r^{w2} \approx 2$ (see equations (9),(10)). This pattern is observed for a wide variety of resonance ratio values of the controlled system. Therefore, the acceleration feedback allows to effectively achieve both sufficient damping and fast reference tracking by virtually shifting the undesirable resonance ratio to its optimal value. We can conclude that even in terms of the optimal control it is acceptable to tune the acceleration gain and the PI controller parameters separately allowing to recover the closed-loop performance achievable for a well behaved system with $r \approx 2$ (Fig. 5).

4.1 Effects of a higher resonance mode

A fundamental question is whether the obtained results hold also for systems with two or more flexible modes and what amount of performance degradation can be expected. This was studied in terms of the optimization problem defined by Figure 4 with the plant formed by the normalized three-mass system (8). The acceleration feedback K_a was tuned to its optimal value by setting $r^w = 2$ in (10) and the PI controller was enhanced by a second-order low-pass Butterworth filter with a cut-off frequency ω_{lp} to improve the high-frequency roll-off allowing a gain-stabilization of the second mode

$$\mathbf{P(s)} = \begin{bmatrix} s \cdot P^l_{n3}(s) & P^m_{n3}(s) \end{bmatrix}^T, \tag{20}$$

$$C_{PI-LP}(s) = \frac{Kp \cdot s + K_i}{s} \cdot \frac{\omega^2_{lp}}{s^2 + 2 \cdot 0.7071 \omega_{lp} s + \omega^2_{lp}}.$$

Representative values of the plant damping factors were selected ($\xi_{z1} = \xi_{z2} = 0.01$, $\xi_{p1} = \xi_{p2} = 0.01 \cdot r_1$). The closed-loop performance criterion is given as

$$\|H\|_\infty = \left\| \begin{bmatrix} W_1(s) S^{ma}_3(s) \\ W_2(s) \cdot s \cdot T^{la}_3(s) \end{bmatrix} \right\|_\infty \leq \gamma, \tag{21}$$

where $S^m_3(s)$ and $T^l_3(s)$ are the sensitivity functions defined analogically to the two-mass system case (with the inner acceleration loop). The weights $W_1(s), W_2(s)$ were fixed to the values used for the two-mass system analysis in the previous section to allow a direct comparison in terms of the achievable γ.

Figure 6 shows the relation of the minimum criterion cost γ depending on the r_2 ratio for different values of r_1 and r_3. It is observed that the performance degradation can be significant with the second resonance mode approaching the first one. The sensitivity to the higher mode increases for low values of the first resonance ratio ($r_1 << 2$) and depends also on the second mode ratio r_3. We can conclude that the technique of virtual resonance ratio shaping in combination with the PI controller can be successfully used even for three-mass systems, provided that the second resonance mode is far enough from the first one. Otherwise, the closed-loop bandwidth has to be reduced or a more complex control strategy is needed. Systems with more than two dominant resonances can be treated in the same manner provided that the feedback controller achieves a sufficient high-frequency roll-off to allow their gain stabilization. This is demonstrated in the following section.

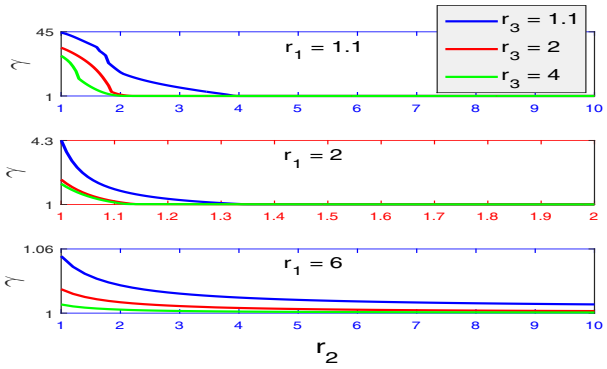

Fig. 6. Criterion cost as a function of r_2 for different values of r_1 and r_3

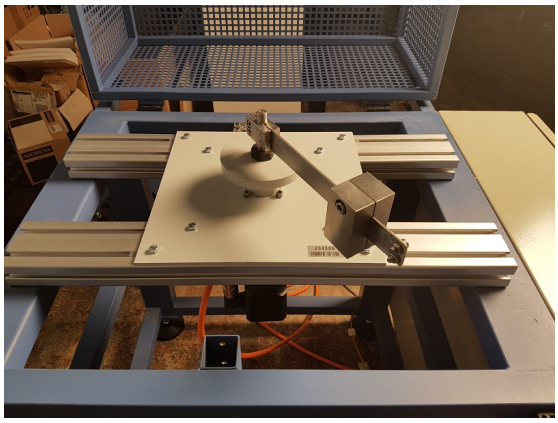

Fig. 7. Mechanical setup used for the experiments

5. EXPERIMENTAL RESULTS

The proposed control design methodology was experimentally verified by means of a mechanical setup consisting of an electrical drive and a flexible mechanical arm (Fig. 7). The system is driven by a 500W permanent magnets synchronous servomotor controlled by a TGDrives frequency inverter which realizes a current control loop. Velocity and position control is implemented in our own developed industrial computer based on Altera Cyclone V System-on-Chip containing two ARM Cortex-A9 CPU cores and a programmable FPGA. The control platform provides real-time EtherCAT communication with the drive with a 2kHz update rate and performs an A/D conversion of the analog signal from the load-attached accelerometer (Kistler piezoceramic, ±50g, 5kHz bandwidth). The ARM cores run a Linux operating system with RT-PREEMT extension. The control algorithms are implemented in REX control system (Balda et al. (2005)).

The flexible arm setup proved to be an excellent benchmark problem for various vibration control methods. It is a distributed parameter system which can exhibit oscillatory behavior with diverse dynamic characteristics and multiple resonance modes allowing emulation of many practical motion control problems. Analytic model of the system can be derived by using a Euler-Bernoulli beam theory (Bernzen (1999)). The system dynamics of a pinned-free flexible beam can be modeled by a partial differential equation

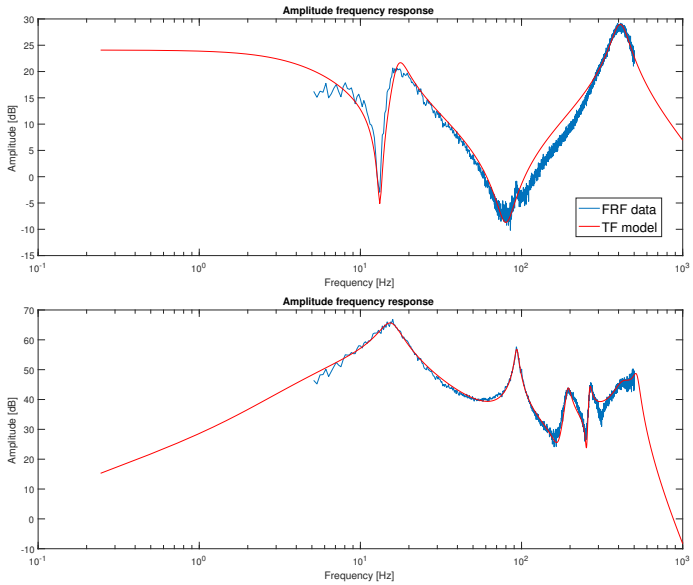

Fig. 8. Identified transfer function models - motor velocity and tip acceleration frequency response

$$\frac{\partial^2}{\partial x^2}(EI(x)\frac{\partial^2 y(x,t)}{\partial x^2}) + \mu\frac{\partial^2 y(x,t)}{\partial t^2} = f(x,t), \qquad (22)$$

where EI is flexural stiffness, μ is distributed mass, $y(x,t)$ is flexible beam deflection and $f(x,t)$ is the sum of all external forces. The equation can be solved by the separation of variables method. Truncation of the high-frequency dynamics by assuming a limited number of orthogonal modes leads to the same model structure as in the case of lumped multi-mass system (1), although the tip dynamics may contain non-minimum phase zeros.

Parameters of the dynamic model were acquired from the experimental identification. A wide-band excitation signal in the form of a pseudo-random binary sequence was injected as a desired motor current. The response of the motor velocity and load acceleration was collected for the subsequent model fitting. A nonparametric estimate of the plant frequency response was acquired by means of the modified Welch method of weighted averaged periodograms (Barbe et al. (2010)). The complex frequency response data were approximated by rational transfer functions by forming a nonlinear least squares minimization of criterion function

$$J = \sum_{k=0}^{M} |\hat{P}(j\omega_k) - P(j\omega_k)|^2, \qquad (23)$$

with respect to the coefficients of the model $P(j\omega)$ and frequency response points $\hat{P}(j\omega_k), k = 0..M$ of the non-parametric model from the previous step. The identified transfer functions for the motor velocity and load acceleration are

$$P_v^m(s) = \frac{\omega_m(s)}{T_m(s)} = \frac{num_1(s)}{den_1(s)}\,\mathrm{e}^{-0.002s},$$
$$P_a^l(s) = \frac{\varepsilon_l(s)}{T_m(s)} = \frac{num_2(s)}{den_2(s)}\,\mathrm{e}^{-0.002s}, \qquad (24)$$

with numerator and denominator polynomials coefficients given by the vectors

$$\begin{aligned} cn_1 &= [8.89e7, 1.02e10, 2.31e13, 1.53e14, 1.54e17],\\ cd_1 &= [1, 4880, 9.54e6, 2.85e10, 1.67e12, 3.45e14, 9.638e15],\\ cn_2 &= [1.55e22, -3.06e25, 6e28, -1.11e32, 5.26e34, -9.13e37, 7.56e39,\\ &\quad -1.09e43, 8.63e45, -8.83e46, 0],\\ cd_2 &= [1, 7197, 4.32e7, 1.72e11, 5.82e14, 1.35e18, 3.17e21, 4.09e24, 7.35e27,\\ &\quad 4.83e30, 6.63e33, 1.83e36, 1.58e39, 1.83e41, 1.99e43, 1.26e45, 2.36e46]. \end{aligned} \qquad (25)$$

The result of the model fitting is shown in Figure 8 which displays the amplitude frequency response of the nonparametric FRF data and parametric transfer function models. Five dominant resonances are observed in the tip dynamics. The first four of them correspond to the lateral and torsional bending modes of the arm whereas the last one is caused by the elasticity of the motor-arm coupling. Only two modes are well observable from the motor side output. There is an additional dynamics caused by a communication delay, current loop lag and analog filtering of the accelerometer signal.

Two different position control schemes were compared to evaluate the potential advantage of the acceleration feedback. The first controller comprised of the traditional P-PI cascade scheme with a second order Butterworth low-pass filter included in the inner velocity loop to provide better high-frequency roll-off. For the second control scheme, the static acceleration feedback was added to shift the resonance ratio of the first mode to the optimal value of $r = 2$. The optimal velocity loop parameters K_p, K_i, ω_{lp} were tuned using the structured H_∞ synthesis with the weighting scheme presented in the previous section (Fig. 4). The position loop gain K_p^p was derived using loop-shaping method aiming at highest achievable bandwidth without an overshoot in the step response and sufficient gain and phase stability margins.

The weights and controller gains for the conventional cascade scheme are

$$W_1(s) = \frac{0.67s + 28.32}{s + 0.028},\ W_2 = 0.011,\ K_a = 0 \qquad (26)$$
$$K_p = 0.055,\ K_i = 1.86,\ \omega_{lp} = 272Hz,\ K_p^p = 8.14.$$

The second controller weights and resulting parameters are given as

$$W_1(s) = \frac{0.67s + 28.32}{s + 0.028},\ W_2 = 0.0094,\ K_a = 2.5e-3 \qquad (27)$$
$$K_p = 0.173,\ K_i = 1.76,\ \omega_{lp} = 133Hz,\ K_p^p = 8.2.$$

Figure 9 shows the comparison of the tracking performance using both control schemes. The motor was commanded to perform a step point-to-point movement. Although the motor side responses looks similar, load side oscillations are observed when using the conventional controller due to the low resonance ratio of the first mode. The acceleration feedback provides much better vibration damping. This is confirmed also by a disturbance rejection test shown in the bottom plot of Fig. 10 where a short pulse of torque (1Nm amplitude, 20ms duration) was injected by the motor during standstill. The improved damping characteristics can also be observed in the identified frequency response from the motor side disturbance to the tip acceleration (Fig. 10 top). The acceleration feedback allows about 12dB better attenuation of the first two flexible modes at the cost of slight amplification of the $3rd$ and $5th$ resonance.

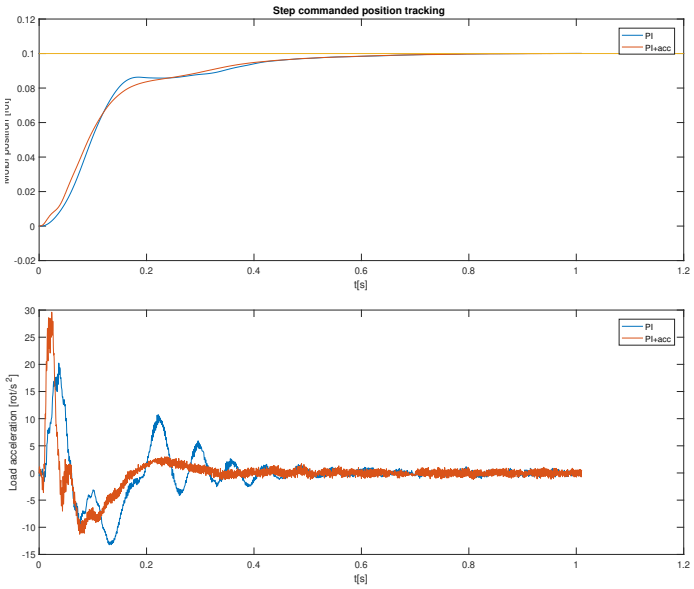

Fig. 9. Comparison of tracking performance

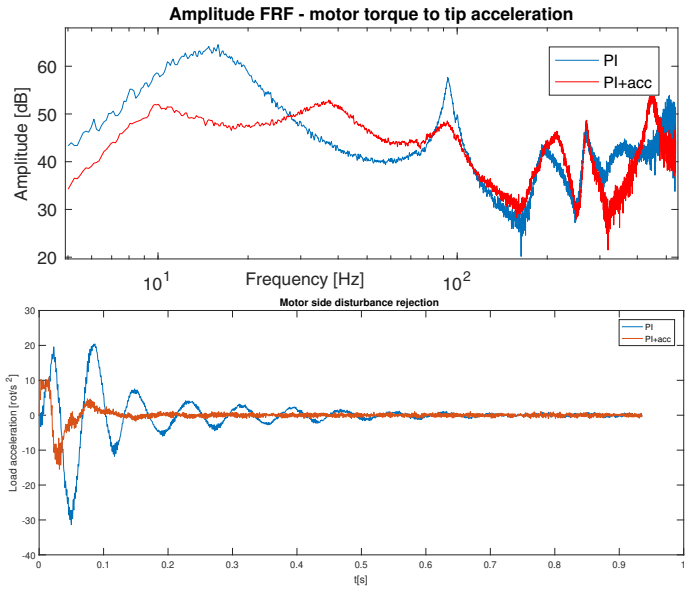

Fig. 10. Comparison of disturbance rejection performance

6. CONCLUSION

The presented results provide an insight on how to employ a complementary load-side acceleration feedback. Closed loop performance of the conventional cascade PID control can be substantially improved. Even a simple static feedback can remove inherent limitations caused by the improper resonance ratio of the first flexible mode. The proposed structured H_∞ optimization can be replaced by an arbitrary design method for PID controllers preceded by the virtual correction of the resonance ratio.

Future research should address potential improvements of dynamic acceleration feedback. Benefits of more complex feedback compensators will also be investigated.

REFERENCES

Axelsson, P., Helmersson, A., and Norrlöf, A. (2014). H-infinity controller design methods applied to one joint of a flexible industrial manipulator. *19th IFAC World Congress*.

Balda, P., Schlegel, M., and Štětina, M. (2005). Advanced control algorithms + Simulink compatibility + real-time OS = REX. In *IFAC World Congress 2005*.

Barbe, K., Pintelon, R., and Schoukens, J. (2010). Welch method revisited: Nonparametric power spectrum estimation via circular overlap. *IEEE Transactions on Signal Processing*.

Bernzen, W. (1999). Active vibration control of flexible robots using virtual spring-damper systems. *Journal of intelligent and robotic systems*, 24.

de Argandona, I.R., Zatarain, M., Illarramendi, A., and Azpeitia, J.L. (2005). Improvement of the performance in machine tools by means of state space control strategies. In *Proceedings of the 44th IEEE Conference on Decision and Control*.

Goubej, M. (2016). Fundamental performance limitations in PID controlled elastic two-mass systems. *IEEE International Conference on Advanced Intelligent Mechatronics*.

Ji, J. and Sul, S. (1995). Kalman filter and LQ based speed controller for torsional vibration suppression in a 2-mass motor drive system. *IEEE Transactions on Industrial Electronics*.

Katsura, S. and Ohnishi, K. (2007). Force servoing by flexible manipulator based on resonance ratio control. *IEEE Transactions on Industrial Electronics*.

Nam, K.T., Lee, S.J., Kuc, T.Y., and Kim, H. (2016). Position and velocity estimation for two-inertia system with nonlinear stiffness based on acceleration sensor. *Sensors 2016, 16, 49*.

Szabat, K. and Orlowska-Kowalska, T. (2007). Vibration suppression in a two-mass drive system using PI speed controller and additional feedbacks - comparative study. *IEEE Transactions on Industrial Electronics*.

Thomsen, S., Hoffmann, N., and Fuchs, F. (2011). PI control, PI-based state space control, and model-based predictive control for drive systems with elastically coupled loads; a comparative study. *IEEE Transactions on Industrial Electronics*.

Watanabe, K., Ito, K., Iwasaki, M., Antonello, R., and Oboe, R. (2016). Estimation of load-side position of two mass resonant systems using MEMS accelerometers. In *2016 IEEE 14th International Workshop on Advanced Motion Control*.

Yuki, K., Murakami, T., and Ohnishi, K. (1993). Vibration control of 2 mass resonant system by resonance ratio control. *International Conference on Industrial Electronics, Control, and Instrumentation*.

Zhang, G. (1999). Comparison of control schemes for two-inertia system. *International Conference on Power Electronics and Drive Systems*.

Zhang, G. (2000). Speed control of two-inertia system by PI/PID control. *IEEE Transactions on Industrial Electronics*.

Zirn, O. and Jaeger, C. (2010). Vibration damping for machine tool servo drives by load acceleration feedback. In *2010 IEEE International Symposium on Industrial Electronics*.